Relations Between Statistics of Three-Dimensional Flame Curvature and its Two-Dimensional Counterpart in Turbulent Premixed Flames

Nilanjan Chakraborty[1] · Raheel Rasool[2] · Umair Ahmed[1] · Markus Klein[2]

Abstract

The relations between the actual flame curvature probability density function (PDF) evaluated in three-dimensions and its two-dimensional counterpart based on planar measurements have been analytically derived subject to the assumptions of isotropy and statistical independence of various angles and two-dimensional curvature. These relations have been assessed based on Direct Numerical Simulation (DNS) databases of turbulent premixed (a) statistically planar and (b) statistically axisymmetric Bunsen flames. It has been found that the analytically derived relation interlinking the PDFs of actual three-dimensional curvature and its two-dimensional counterpart holds reasonably well for a range of curvatures around the mean value defined by the inverse of the thermal flame thickness for different turbulence intensities across different combustion regimes. The flame surface is shown to exhibit predominantly two-dimensional cylindrical curvature but there is a significant probability of finding saddle type flame topologies and this probability increases with increasing turbulence intensity. The presence of saddle type flame topologies affects the ratios of second and third moments of two-dimensional and three-dimensional curvatures. It has been demonstrated that the ratios of second and third moments of two-dimensional and three-dimensional curvatures cannot be accurately predicted based on two-dimensional measurements. The ratio of the third moments of two-dimensional and three-dimensional curvatures remains positive and thus the qualitative nature of curvature skewness can still be obtained based on two-dimensional curvature measurements. As the curvature skewness is often taken to be a marker of the Darrius-Landau instability, the conclusion regarding the presence of this instability can potentially be taken from the two-dimensional curvature measurements.

✉ Markus Klein
  markus.klein@unibw.de

1   School of Engineering, Newcastle University, Claremont Road, Newcastle NE1 7RU, UK

2   Department of Aerospace Engineering, University of the Bundeswehr Munich, Werner-Heisenberg-Weg 39, 85577 Neubiberg, Germany

1 Introduction

The statistics of flame curvature are fundamentally important for the physics of turbulent premixed flame propagation (Poinsot and Veynante 2001) and from the point of view of the development of models (Bradley et al. 2003; Hawkes and Cant 2000; Chakraborty and Cant 2007). It is well-known that the flame curvature affects the local flame displacement speed in turbulent premixed combustion (Peters et al. 1998; Chakraborty and Cant 2004; Chakraborty 2007). Moreover, the presence of the flame curvature induces additional stretch rate which plays a key role in determining the evolutions of Flame Surface Density (FSD) (Chakraborty and Cant 2007, 2009) and Scalar Dissipation Rate (SDR) (Chakraborty et al. 2011a) in the context of turbulent premixed combustion modelling. It was suggested in the premixed combustion literature that the negative skewness of the curvature probability density function (PDF) can be a marker of the Darrieus-Landau type instability in turbulent premixed flames (Creta et al. 2016; Klein et al. 2018a). From the foregoing it can be appreciated that the distribution of curvature is an important quantity for experimental measurements (Shepherd and Ashurst 1992; Shy et al. 2000; Shepherd and Cheng 2001; Chen and Bilger 2002; Lachaux et al. 2005; Gashi et al. 2005; Anselmo-Filho et al. 2009; Renou et al. 1998). In experimental diagnostics of turbulent premixed combustion, flame location and flame wrinkling are usually measured by Rayleigh scattering, Planar Laser Induced Fluorescence (PLIF) and tomography of small vaporising droplets (Shepherd and Ashurst 1992; Shy et al. 2000; Shepherd and Cheng 2001; Chen and Bilger 2002; Lachaux et al. 2005; Gashi et al. 2005; Anselmo-Filho et al. 2009; Renou et al. 1998). However, to date, most experimental measurements of curvature depend upon two-dimensional measurements (Shepherd and Ashurst 1992; Shy et al. 2000; Shepherd and Cheng 2001; Chen and Bilger 2002; Lachaux et al. 2005; Gashi et al. 2005; Anselmo-Filho et al. 2009; Renou et al. 1998). Although it has been demonstrated through previous Direct Numerical Simulation (DNS) data that even though the flame surface predominantly shows two-dimensional cylindrical curvature, the relative alignment of the approximately cylindrical surface with the measurement plane at the time of measurement cannot be ascertained. As a result, two-dimensional measurements of curvature may not offer true reflection of the actual flame curvature evaluated in three-dimensions, and this was demonstrated previously based on DNS data (Chakraborty et al. 2011b). It is now possible to conduct three-dimensional measurements of the relevant quantities at the intersection lines of two intersecting planes (Steinberg and Driscoll 2009; Chen et al. 2007; Shy et al. 1999), and from liquid autocatalytic reaction fronts (Knaus et al. 2005). These methods are still extremely expensive, and two-dimensional measurements are expected to be the widely used methodology in the foreseeable future. For this purpose, a correction methodology which approximates the probability density functions (PDFs) of the actual flame curvature in three-dimensions from the PDFs of curvature measured in two-dimensions will be beneficial for the purpose of application of experimental measurements from the point of view of model development and assessment (Bradley et al. 2003; Hawkes and Cant 2000; Chakraborty and Cant 2004, 2007; Echekki and Chen 1996; Peters et al. 1998; Chakraborty 2007). This aspect has been addressed in this paper by deriving an analytical expression which relates the PDFs of two-dimensional curvature with the PDFs of actual flame curvature under certain assumptions (e.g., isotropy of the flame normal vector). The applicability of the analytically derived expression to relate the PDFs of two-dimensional and three-dimensional (i.e., actual) curvatures has been assessed by considering three-dimensional Direct Numerical Simulation (DNS) databases of turbulent premixed statistically planar

and axisymmetric Bunsen flames. This DNS data has been utilised to directly evaluate the flame curvature in three-dimensions, whereas the two-dimensional curvature is evaluated based on scalar distributions on two-dimensional planes containing the mean direction of flame propagation. In this regard, the main objectives of this paper are: (1) to present a theoretical framework which enables extraction of the PDFs of actual curvature evaluated in three-dimensions from the PDFs of the curvature extracted from two-dimensional measurements, (2) to assess the applicability of the theoretical framework by extracting flame curvatures in both two- and three-dimensions from DNS data of statistically planar flames and Bunsen flames for a range of different turbulence intensities and combustion regimes.

2 Mathematical background

The mean value of two principal curvatures (i.e., κ_1 and κ_2) is commonly referred to as flame curvature, which is defined as:

$$\kappa_m = 0.5(\kappa_1 + \kappa_2) = 0.5\nabla \cdot \vec{N} \tag{1}$$

where $\vec{N}$ is the flame normal vector. The flame normal vector $\vec{N}$ is defined as: $\vec{N} = -\nabla c/|\nabla c|$, where c is the reaction progress variable which increases monotonically from 0.0 in the unburned gas to 1.0 in fully burned products. The reaction progress variable c can be defined in terms of a suitable species mass fraction Y_m as: $c = (Y_{m0} - Y_m)/(Y_{m0} - Y_{m\infty})$ with subscripts 0 and ∞ representing the values in pure reactants and fully burned products, respectively. The evaluation of κ_m depends on the evaluation of all three components of ∇c (i.e. $\partial c/\partial x_1$, $\partial c/\partial x_2$, $\partial c/\partial x_3$) but all of these components are not available in two-dimensional measurements. For the subsequent discussion, it is important to refer to Fig. 1 where the brown surface is considered to represent the flame surface, whereas the measurement surface and tangent plane passing through point A are shown in blue and grey colours, respectively. The angles and coordinate systems without the obstruction of the flame surface are shown in Fig. 1b.

The laboratory coordinate system (shown with red arrows) is represented by the orthogonal system $\vec{b}$ such that the $b_1 - b_2$ plane is the measurement plane and $\vec{b_3}$ is the out of plane direction. The distances in $\vec{b_1}$ and $\vec{b_2}$ directions are given by y_{b1} and y_{b2} and ϕ is the angle between the flame normal vector $\vec{N}$ and the measurement plane. Based on $\partial c/\partial y_{b1}$ and $\partial c/\partial y_{b2}$, it is possible to obtain the two-dimensional curvature in the following manner:

$$k_2 = 0.5\left\{\frac{\partial}{\partial y_{b1}}\left[-\frac{(\partial c/\partial y_{b1})}{\sqrt{(\partial c/\partial y_{b1})^2 + (\partial c/\partial y_{b2})^2}}\right] + \frac{\partial}{\partial y_{b2}}\left[-\frac{(\partial c/\partial y_{b2})}{\sqrt{(\partial c/\partial y_{b1})^2 + (\partial c/\partial y_{b2})^2}}\right]\right\} \tag{2}$$

Consider a second point A' within a small distance of A located on the magenta intersecting line. If h_3 is the height of A' above the tangent plane (see Fig. 1b), it can be shown that (Hawkes et al. 2011; Veynante et al. 2010; Chakraborty and Hawkes 2011; Chakraborty et al. 2013; Wang et al. 2021):

$$h_3 = 0.5\kappa_1 y_{e1}^2 + 0.5\kappa_2 y_{e2}^2 \tag{3}$$

Fig. 1 **a** Flame surface, tangent plane and measurement plane **b** Coordinates and reference frames used in this analysis

(a)

(b)
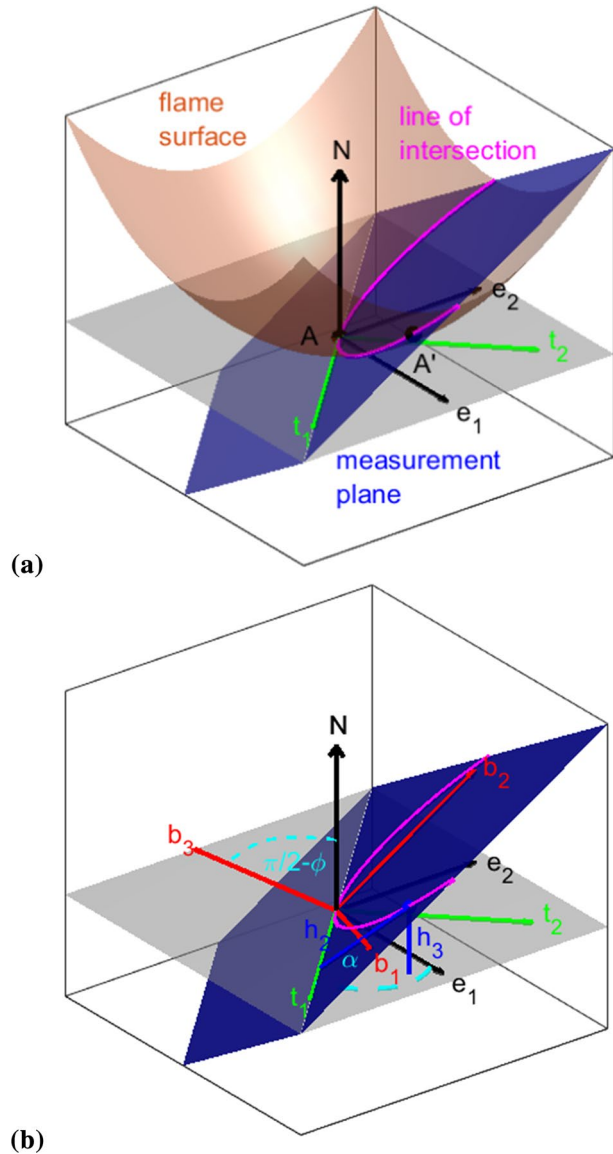
where y_{e1} and y_{e2} are distances in the principal directions $\vec{e_1}$ and $\vec{e_2}$ corresponding to principal curvatures κ_1 and κ_2 in the tangent plane at the point A. Figure 1 suggests that the measured height h_2 above the tangent t_1 in the two-dimensional plane can be expressed as (Hawkes et al. 2011; Veynante et al. 2010; Chakraborty and Hawkes 2011; Chakraborty et al. 2013; Wang et al. 2021):

$$h_2 \cos \phi = h_3 \tag{4}$$

Here t_1 and t_2 is an orthogonal coordinate system in the tangent plane such that t_1 lies both in the measurement and tangent plane. If the angle between t_1 and e_1 is taken to be

α, it is possible to write the distances y_{e1} and y_{e2} as (Hawkes et al. 2011; Veynante et al. 2010; Chakraborty and Hawkes 2011; Chakraborty et al. 2013; Wang et al. 2021):

$$y_{e1} = y_{t1} \cos \alpha + y_{t2} \sin \alpha \quad \text{and} \quad y_{e2} = -y_{t1} \sin \alpha + y_{t2} \cos \alpha \tag{5}$$

where y_{t1} and y_{t2} are the distances in the $\vec{t}$ coordinate system. Using Eqs. (2)–(5), it is possible to write the following relation for $k_2 = 0.5 \partial^2 h_2 / \partial y_{t_1}^2$ (Hawkes et al. 2011; Veynante et al. 2010; Chakraborty and Hawkes 2011; Chakraborty et al. 2013; Wang et al. 2021):

$$2k_2(\cos \phi) = \kappa_1(\cos^2 \alpha) + \kappa_2(\sin^2 \alpha) \tag{6}$$

Taking derivative on both sides yields:

$$2dk_2(\cos \phi) = \left[d\kappa_1(\cos^2 \alpha) + d\kappa_2(\sin^2 \alpha) + 2k_2(\sin \phi)d\phi + (\kappa_2 - \kappa_1)(\sin 2\alpha)d\alpha \right] \tag{7}$$

By considering ϕ, α and k_2 statistically independent, it is possible to express the joint PDF of ϕ, α and k_2 (i.e. $P(\phi, \alpha, k_2)$) as $P(\phi, \alpha, k_2) = P(\phi)P(\alpha)P(k_2)$, which upon multiplying both sides of Eq. (7) yields:

$$
\begin{aligned}
2(\cos \phi)P(\phi)P(\alpha)P(k_2)dk_2 = &[d\kappa_1(\cos^2 \alpha) + d\kappa_2(\sin^2 \alpha) \\
&+ 2k_2(\sin \phi)d\phi + (\kappa_2 - \kappa_1) \\
&(\sin 2\alpha)d\alpha]P(\phi)P(\alpha)P(k_2)
\end{aligned}
\tag{8}
$$

It is possible to assume an isotropic distribution of ϕ if the probability of finding an angle ϕ within the differential change of angle $d\phi$ is assumed to be proportional to the area swept on a unit sphere defining all possible orientations of flame normal vector $\vec{N}$. Therefore, the PDF of ϕ is assumed as (Hawkes et al. 2011; Veynante et al. 2010; Chakraborty and Hawkes 2011; Chakraborty et al. 2013; Wang et al. 2021): $P(\phi) = (\cos \phi)/2$. A uniform distribution was assumed for α in previous studies (Hawkes et al. 2011; Veynante et al. 2010; Chakraborty and Hawkes 2011; Chakraborty et al. 2013; Wang et al. 2021), which alongside Eq. (8) yields:

$$
\begin{aligned}
&\int_{-\infty}^{\infty} \int_{\alpha=-\pi}^{\alpha=\pi} \int_{\phi=-\pi/2}^{\phi=\pi/2} \cos^2 \phi P(\alpha)P(k_2)d\phi d\alpha dk_2 = \\
&(1/2\pi)\int_{-\infty}^{\infty} \int_{\alpha=-\pi}^{\alpha=\pi} \int_{\phi=-\pi/2}^{\phi=\pi/2} \left[(\cos^2 \alpha)d\kappa_1 + (\sin^2 \alpha)d\kappa_2\right]P(\phi)P(k_2)d\phi d\alpha
\end{aligned}
\tag{9}
$$

It is worth noting the other terms on the right hand side of Eq. (8) do not appear in Eq. (9) because $\int_{\phi=-\pi/2}^{\phi=\pi/2} (\sin \phi \cos \phi)d\phi = 0$ and $\int_{\alpha=-\pi}^{\alpha=\pi} (\sin 2\alpha)d\alpha = 0$. It is worth noting that the expressions of $P(\phi) = (\cos \phi)/2$ and $P(\alpha) = 1/2\pi$ are used here based on the assumed isotropic distribution of the flame normal vector $\vec{N}$ for the purpose of simplification of the mathematical derivation. These assumptions were made in several previous studies (Hawkes et al. 2011; Veynante et al. 2010; Chakraborty and Hawkes 2011; Chakraborty et al. 2013; Wang et al. 2021) which proposed correction factors for the planar measurements of the FSD and scalar dissipation rate transport equations to obtain their actual three-dimensional counterparts. On top of these assumptions,

statistical independence is assumed for ϕ, α and k_2 (i.e. $P(\phi, \alpha, k_2) = P(\phi)P(\alpha)P(k_2)$) for the sake of obtaining a derivation of a simple analytical expression relating $P(k_2)$ and $P(\kappa_m)$.

Using $\int_{\phi=-\pi/2}^{\phi=\pi/2} \cos^2 \phi d\phi = \pi/2$, $\int_{\alpha=-\pi}^{\alpha=\pi} (\cos^2 \alpha)/2\pi d\alpha = 1/2$ and

$\int_{\alpha=-\pi}^{\alpha=\pi} (\sin^2 \alpha)/2\pi d\alpha = 1/2$, it is possible to obtain:

$$\int_{-\infty}^{\infty} P(k_2)dk_2 = \int_{-\infty}^{+\infty} (2/\pi)P(k_2)d\kappa_m = 1.0 = \int_{-\infty}^{+\infty} P(\kappa_m)d\kappa_m \qquad (10)$$

Equation (10) suggests:

$$P(k_2)dk_2 = P(\kappa_m)d\kappa_m \quad \text{and} \quad P(\kappa_m) = (2/\pi)P(k_2) \qquad (11)$$

A correction factor for the two-dimensional curvature PDF similar to Eq. (11) was previously empirically used in Refs. (Chakraborty et al. 2011b; Wang et al. 2021) but no theoretical justification was provided. The above derivation provides the theoretical justification for a relation between the PDFs of actual flame curvature and its two-dimensional counterpart for the first time. Moreover, it is worth investigating if Eq. (11) is sufficient to predict the higher moments of curvature based on two-dimensional measurements. In order to assess this aspect, Eqs. (6) and (11) are used along with $P(\phi) = (\cos \phi)/2$ and $P(\alpha) = 1/2\pi$ to yield:

$$\overline{k_2^2} = \int_{-\infty}^{\infty} k_2^2 P(k_2)dk_2 = \frac{3}{8}\left[\frac{3}{2}\int_{-\infty}^{\infty} \kappa_m^2 P(\kappa_m)d\kappa_m - \frac{1}{2}\int_{-\infty}^{\infty} \kappa_1\kappa_2 P(\kappa_m)d\kappa_m\right] \qquad (12i)$$

$$\overline{k_2^3} = \int_{-\infty}^{\infty} k_2^3 P(k_2)dk_2 = \frac{2}{3\pi}\left[\frac{5}{2}\int_{-\infty}^{\infty} \kappa_m^3 P(\kappa_m)d\kappa_m - \frac{3}{2}\int_{-\infty}^{\infty} \kappa_1\kappa_2\kappa_m P(\kappa_m)d\kappa_m\right] \qquad (12ii)$$

Equations (12i) and (12ii) can be rewritten as:

$$\overline{k_2^2}/\overline{\kappa_m^2} = \frac{9}{16}\left[1 - \frac{1}{3}\left(\overline{\kappa_m^2}\right)^{-1}\int_{-\infty}^{\infty} \kappa_1\kappa_2 P(\kappa_m)d\kappa_m\right] \qquad (13i)$$

$$\overline{k_2^3}/\overline{\kappa_m^3} = \frac{5}{3\pi}\left[1 - \frac{3}{5}\left(\overline{\kappa_m^3}\right)^{-1}\int_{-\infty}^{\infty} \kappa_1\kappa_2\kappa_m P(\kappa_m)d\kappa_m\right] \qquad (13ii)$$

where $\int_{-\infty}^{\infty} \kappa_m^2 P(\kappa_m)d\kappa_m = \overline{\kappa_m^2}$ and $\int_{-\infty}^{\infty} \kappa_m^3 P(\kappa_m)d\kappa_m = \overline{\kappa_m^3}$. It has been demonstrated in previous analyses (Chakraborty and Cant 2006; Cifuentes et al. 2019; Chakraborty et al. 2020) that the premixed flame surface shows significant probability of saddle type (i.e., $\kappa_1\kappa_2 < 0$) flame topology and thus $\overline{k_2^2}/\overline{\kappa_m^2}$ and $\overline{k_2^3}/\overline{\kappa_m^3}$ are expected to assume values greater than $9/16 = 0.5625$ and $5/3\pi = 0.5305$, respectively.

## 3 Numerical implementation

The validity of Eq. (11) is assessed in this paper based on existing three-dimensional DNS databases of statistically planar (Ahmed et al. 2019a, b, 2021) and statistically axisymmetric Bunsen (Klein et al. 2018a, b; Chakraborty et al. 2019) turbulent premixed flames. A single step Arrhenius type irreversible chemical reaction is considered for these simulations. This simplification of chemistry allows for an extensive parametric analysis. As the mathematical derivation in Sect. 2 is independent of the choice of chemical mechanism, the simplification of chemistry is not expected to play a key role in the assessment of the expressions given by Eqs. (11) and (13). It was demonstrated in a recent analysis (Keil et al. 2021) that the PDFs of tangential diffusion component of displacement speed (i.e. $S_t = -2D\kappa_m$ where D is the reaction progress variable diffusivity) for both simple and detailed chemistry DNS are both qualitatively and quantitatively similar. As D does not vary significantly for a given value of c, the qualitative and quantitative similarities of S_t PDFs imply the same for the PDFs of curvature κ_m. Therefore, the outcomes of simple chemistry DNS based assessments of curvature statistics are expected to hold for detailed chemistry simulations.

The simulations have been conducted using the compressible DNS code SENGA + (Klein et al. 2018a, b; Ahmed et al. 2019a, b, 2021; Chakraborty et al. 2019; Keil et al. 2021; Jenkins and Cant 1999) where the conservation equations of mass, momentum, energy, and species are solved in non-dimensional form. All the spatial derivatives in SENGA + are approximated using a 10th order central difference scheme for the internal grid points, but the order of accuracy gradually drops to a one-sided 2nd order scheme at the non-periodic boundaries. The temporal advancement is carried out using an explicit 3rd order Runge–Kutta scheme. The Navier–Stokes Characteristic Boundary Conditions (NSCBC) (Poinsot and Lele 1992) have been used to specify turbulent inflow and partially non-reflecting outflow boundaries in the direction of mean flame propagation (here taken to be the x_1-direction) and transverse boundaries (i.e., x_2 and x_3 directions) are considered to be periodic for statistically planar turbulent premixed flames. The mean inlet velocity U_{mean} for statistically planar flames is gradually modified to match the turbulent flame speed to ensure a statistically stationary state of the flame. The simulation domain for statistically planar turbulent premixed flames is taken to be $79.5\delta_{th} \times (39.8\delta_{th})^2$, which is discretised by a uniform Cartesian grid of $800 \times 400 \times 400$ with $\delta_{th} = (T_{ad} - T_0)/\max |\nabla T|_L$ being the thermal flame thickness where T, T_0 and T_{ad} are the dimensional temperature, unburned gas temperature and the adiabatic flame temperature, respectively. The root-mean-square turbulent velocity fluctuation normalised by the unstrained laminar burning velocity u'/S_L, integral length scale to thermal flame thickness ratio l/δ_{th} are listed in Table 1 along with the values of Damköhler number $Da = lS_L/u'\delta_{th}$ and Karlovitz number $Ka = (u'/S_L)^{3/2}(l/\delta_{th})^{-1/2}$. The statistically planar flame cases considered in this analysis are shown on the Borghi-Peters diagram (Peters 2000) in Fig. 2, which reveals that these cases range from the corrugated flamelets regime to the thin reaction zones regime and represent a wide range of turbulence intensities. A bandwidth filtered forcing method (Klein et al. 2017) in physical space has been employed for the unburned gas forcing ahead of the flame, which maintains the prescribed turbulence intensity u'/S_L and the desired value of l/δ_{th}. The total simulation time for all statistically planar flame cases remains greater than one throughpass time and at least 10 eddy turnover times (i.e., $10l/u'$) to ensure a statistically steady state in all cases. Interested readers are referred to Chakraborty et al. 2020; Ahmed et al. 2019a) for further information on this dataset.

Table 1 The attributes of the DNS databases considered for this analysis

Statistically planar flame cases

Cases	u'/S_L	l/δ_{th}	Da	Ka	Regime
AP ($P/P_0 = 1.0$)	1.0	3.0	3.0	0.58	Corrugated flamelets
CP ($P/P_0 = 1.0$)	5.0	3.0	0.6	6.5	Thin reaction zones
EP ($P/P_0 = 1.0$)	10.0	3.0	0.3	18.3	Thin reaction zones

Bunsen burner cases with $U_B/S_L = 6.0$

Cases	u'_{inlet}/S_L	l/δ_{th}	Da	Ka	Regime
AB ($P/P_0 = 1.0$)	1.0	5.20	5.0	0.45	Wrinkled/Corrugated flamelets
CB ($P/P_0 = 10.0$)	1.0	16.13	16.13	0.25	Wrinkled/Corrugated flamelets
DB ($P/P_0 = 1.0$)	3.10	5.20	1.67	2.40	Thin reaction zones

The first character to the names used in previous papers (Klein et al. 2018a; Ahmed et al. 2019a; Chakraborty et al. 2019) and P and B refer to statistically planar and Bunsen premixed flames, respectively

Fig. 2 The cases considered on the Borghi-Peters regime diagram
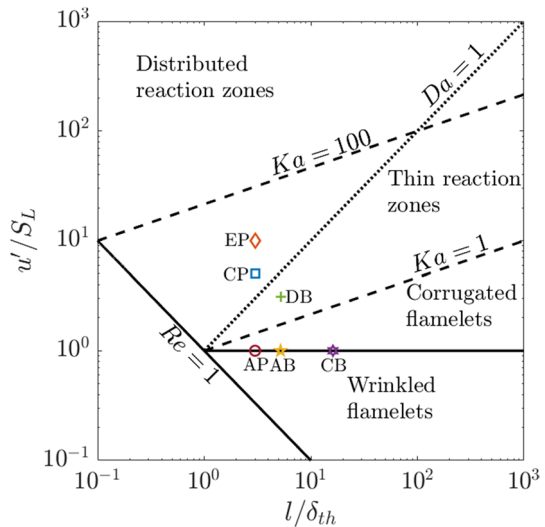
For the turbulent premixed Bunsen flame configuration, the axial direction is taken to align with x_1-direction. All the boundaries apart from the inlet are taken to be partially non-reflecting and are specified using the NSCBC technique (Poinsot and Lele 1992). A mean velocity distribution with a hyperbolic tangent like profile is specified on the inlet. Turbulent velocity fluctuations are then superimposed on this mean profile by generating velocity fluctuations using a modified version (Chakraborty et al. 2019) of the method suggested in Klein et al. (2003), replacing the Gaussian filter with an autoregressive AR1 process in the axial direction. The reacting scalars have been initialised with an unstrained premixed laminar flame solution having the form of a hemisphere with its centre coinciding with that of the inlet. The reaction progress variable c within

the nozzle is taken to be 0.0, whereas the reaction progress variable c outside the nozzle on the inlet boundary plane is taken to be 1.0. No pilot flame is explicitly simulated and can be considered to be placed upstream of the nozzle. The same approach was previously adopted by Poinsot et al. (1992) and Sankaran et al. (2007) for their DNS of premixed Bunsen flames. The computational domain is taken to be a cube with each side equalling to $2d_n$ where d_n is the diameter of the nozzle, which is discretised using a uniform Cartesian grid of dimension $250 \times 250 \times 250$ for Bunsen flames at atmospheric pressure (i.e. $P/P_0 = 1.0$), whereas a grid of size $795 \times 795 \times 795$ is used for the Bunsen flame at the elevated pressure (i.e. $P/P_0 = 10.0$). For the thermochemistry used for Bunsen flame configuration, the domain size for $P/P_0 = 1.0$ ($P/P_0 = 10.0$) cases corresponds to $50\delta_{th} \times 50\delta_{th} \times 50\delta_{th}$ ($159\delta_{th} \times 159\delta_{th} \times 159\delta_{th}$). The normalised mean inflow velocity U_B/S_L, normalised root-mean-square inlet velocity u'_{inlet}/S_L and normalised integral length scale of turbulence (l/δ_{th}) are listed along with inlet values of Damköhler number $Da = lS_L/u'_{inlet}\delta_{th}$ and Karlovitz number $Ka = \left(u'_{inlet}/S_L\right)^{1.5}\left(l/\delta_{th}\right)^{-0.5}$ in Table 1. These cases are also shown in Fig. 2, which reveals that these Bunsen flame cases also range from the corrugated flamelets regime to the thin reaction zones regime on Borghi-Peters regime diagram (Peters 2000). The flame height remains smaller than $2d_n$ for all cases (e.g. the highest flame height is obtained for case AB, which is about $1.5d_n$) and all boundaries other than the inlet plane are taken to be partially non-reflecting so the domain length is not expected to influence the results considered here. All statistics presented in this paper for Bunsen flames are recorded after at least two flow through and two initial eddy turnover times. Interested readers are referred to Klein et al. (2018a, b); Chakraborty et al. (2019) for further information on this database.

For all cases, the heat release parameter is taken to be $\tau = \left(T_{ad} - T_0\right)/T_0 = 4.5$. Standard values are taken for Prandtl number (i.e., $Pr = 0.7$), Zel'dovich number (i.e., $\beta = T_{ac}\left(T_{ad} - T_0\right)/T_{ad}^2 = 6.0$ with T_{ac} being the activation temperature) and the ratio of specific heats (i.e., $\gamma = 1.4$). The grid spacing ensures resolution of both δ_{th} and the Kolmogorov length scale η. It has been found that both the laminar burning velocity and thermal flame thickness did not change appreciable ($<1\%$) by reducing the grid spacing by a factor of 2. Therefore, it can be expected that the curvature statistics are adequately resolved in these simulations. It has also been ensured that the flames in all cases remain sufficiently away from the domain boundaries, so no uncertainty/error affects the curvature statistics extracted from DNS data due to the domain size.

4　Results and discussion

The instantaneous isosurfaces of c for all cases in Table 1 are shown in Fig. 3, which indicates that the flame morphology changes, and the flame becomes increasingly wrinkled with increases in turbulence intensity u'/S_L (for both statistically planar and Bunsen flame cases) and thermodynamic pressure (for Bunsen flame cases). This is reflected in the increases in both turbulent burning velocity and flame surface area and these variations have been presented elsewhere (Ahmed et al. 2019a; Chakraborty et al. 2019) and thus are not repeated here. The PDFs of the normalised curvature $\kappa_m \times \delta_{th}$ for the $c = 0.8$ isosurface for cases AP, CP and EP are exemplarily shown in Fig. 4, respectively along with the PDFs of the corresponding normalised two-dimensional curvature $k_2 \times \delta_{th}$. The maximum reaction rate for the present thermo-chemistry is obtained for $c \approx 0.8$ and thus the $c = 0.8$ isosurface can be taken to be the flame surface. In this paper, the values of curvature from
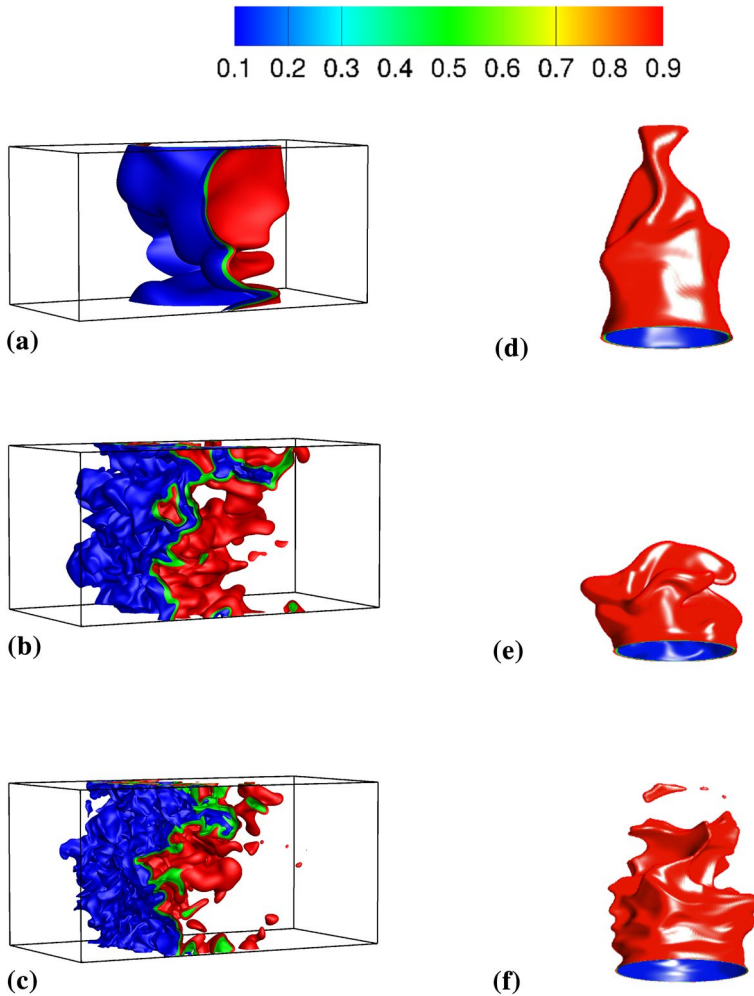
Fig. 3 Isosurfaces of c in **a**–**c** cases AP, CP, EP and **d**–**f** AB, CB, DB under quasi-stationary state

the neighbourhood grid points of the $c = 0.8$ isosurface are interpolated to obtain κ_m and k_2 values at $c = 0.8$ and about 50 bins are kept within the range given by $1 \geq \kappa_m \times \delta_{th} \geq -1$ and $1 \geq k_2 \times \delta_{th} \geq -1$ for constructing the PDFs. The two-dimensional curvature k_2 for the statistically planar flames is evaluated using the contours of $c = 0.8$ in $x_1 - x_2$ and $x_1 - x_3$ planes using Eq. (2), and the results obtained in $x_1 - x_2$ and $x_1 - x_3$ planes are ensemble averaged because these two planes are statistically equivalent. In fact, the PDFs of $k_2 \times \delta_{th}$ obtained from $x_1 - x_2$ planes are almost identical to that evaluated using $x_1 - x_3$ planes and thus are not explicitly shown here. The two-dimensional curvature statistics for cases AB, CB and DB are taken from midplanes containing the x_1-direction, which are statistically equivalent to each other. It is worth noting that the mean value of two-dimensional curvature in the statistically equivalent midplanes for cases AB, CB and DB remains small. Therefore, the statistics for the Bunsen cases AB, CB and DB are shown in Fig. 4 for normalised curvature fluctuations with respect to the mean values (which are evaluated by
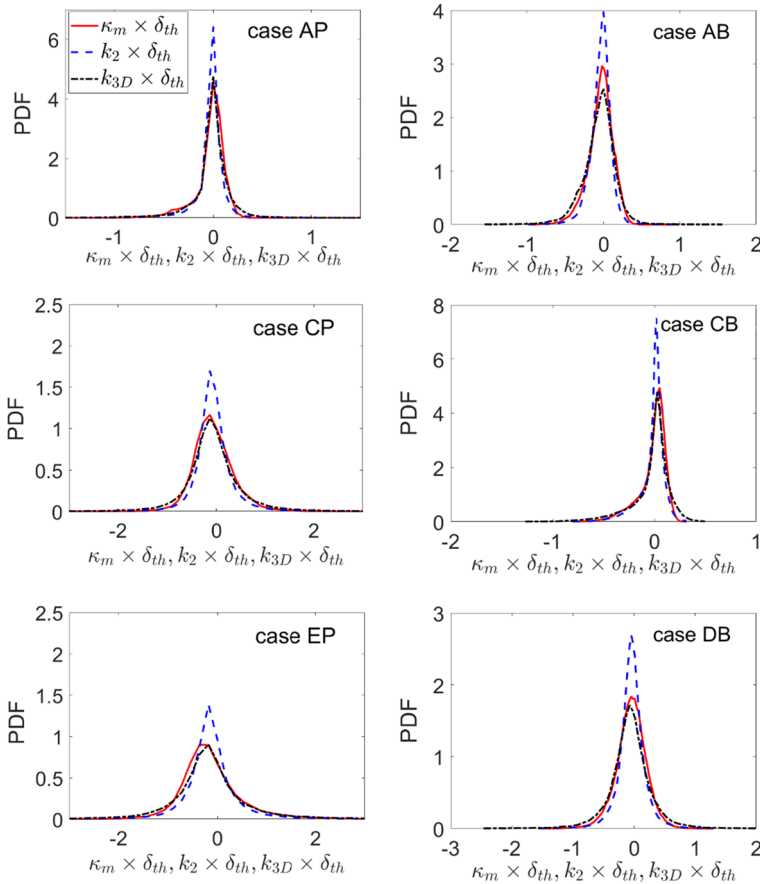
Fig. 4 PDFs of $\kappa_m \times \delta_{th}$, $k_2 \times \delta_{th}$ and $k_{3D} \times \delta_{th} = k_2 \times \pi/2 \times \delta_{th}$ on the $c = 0.8$ isosurface for all cases in linear scale

averaging in time and also in the azimuthal direction) for the purpose of comparison with the statistically planar flame cases. Therefore, κ_m and k_2 will henceforth be understood as the three-dimensional curvature fluctuations and its corresponding two-dimensional evaluation only for turbulent Bunsen flame cases (i.e., cases AB, CB and DB).

It can be seen from Fig. 4 that the PDFs of $\kappa_m \times \delta_{th}$ and $k_2 \times \delta_{th}$ peak around zero values and exhibit significant skewness for small values of u'/S_L in the planar flame case (e.g., case AP) and also for the high pressure Bunsen fame case (e.g., case CB), but the PDFs become increasingly symmetric with increasing turbulence intensity and also with a decrease in thermodynamic pressure for the Bunsen flame cases. The negative skewnesses in cases AP and CB arise due to Huygens propagation and Darrieus-Landau instability respectively, and interested readers are referred to Klein et al. (2018a); Chakraborty et al. (2019) for further information. However, the PDFs of both $\kappa_m \times \delta_{th}$ and $k_2 \times \delta_{th}$ indicate vanishingly small mean values for all cases, which is consistent with the geometry of the statistically planar flames and curvature fluctuation definition for Bunsen flames. It is evident from Fig. 4 that the PDFs of normalised two-dimensional curvature $k_2 \times \delta_{th}$ exhibit sharper peaks and smaller spread in comparison to the corresponding PDFs of the

normalised three-dimensional curvature $\kappa_m \times \delta_{th}$, which is consistent with previous findings (Chakraborty et al. 2011b). These results are also valid for other c isosurfaces across the flame front for all cases considered (not shown here). In order to explain this behaviour, it is useful to consider the statistical distribution of the curvature shape factor s_h, which is defined as $\kappa_{min}/\kappa_{max}$, where κ_{min} is the smaller of κ_1 and κ_2 by magnitude and κ_{max} is the other. The shape factor $s_h = 1.0$ corresponds to spherical curvatures, whereas $s_h = -1.0$ indicates spherical saddle points. The shape factor of $s_h = 0.0$ corresponds to locally cylindrical two-dimensional surfaces. It is worth noting that the joint PDFs of $\kappa_m = 0.5(\kappa_1 + \kappa_2)$ and Gauss curvature $\kappa_1\kappa_2$ for c isosurfaces have been found to be qualitatively similar to that presented elsewhere (Cifuentes et al. 2019) and thus are not repeated here.

The PDFs of s_h for the $c = 0.8$ isosurface for the selected cases are shown in Fig. 5, which shows that the probability of finding spherical curvature (i.e., $s_h = 1.0$) is vanishingly small in all cases. Moreover, the PDFs of s_h in all cases peak at $s_h = 0.0$ indicating the predominance of the two-dimensional locally cylindrical surfaces. There is a significant probability of finding saddle type flame topologies (i.e. $s_h < 0$), which is also consistent with previous findings based on simple (Chakraborty and Cant 2006) and detailed chemistry (Chakraborty et al. 2020) DNS. Considering the predominance of locally cylindrical flame surface, it can be expected that the intersection of the measurement plane with a cylindrical surface gives rise to elliptic sections with radius of curvatures larger than the radius of the cylinder, which ultimately yields a higher probability of finding small curvature magnitudes for two-dimensional measurements. This, in turn, yields a higher maximum value of the PDF of k_2 than that of κ_m, as demonstrated in Fig. 4. However, it is possible to have large magnitudes of k_2 in the limit of $\phi = \pm\pi/2$, and therefore the PDFs of k_2 show both long positive and negative tails (see later in Fig. 6). Thus, the actual distribution of the flame curvature κ_m cannot be obtained from the two-dimensional curvature measurements. Based on Eq. (11) it is possible to define a transformed three-dimensional equivalent curvature k_{3D} from k_2 as:

$$k_{3D} = k_2 \times \pi/2 \qquad (14)$$

Figure 4 shows that the PDFs of $k_{3D} = k_2 \times \pi/2$ satisfactorily capture the maximum values of the PDFs of κ_m according to the transformation suggested by Eq. (11) and capture the general shape of the PDFs of κ_m better than the PDFs of k_2. The same behaviour is obtained for different c isosurfaces across the flame for all cases considered here (not shown for brevity). However, there are some mismatches between the widths of the PDFs of k_{3D} and κ_m. It can be seen from Fig. 6 that there is a considerable mismatch at the tails of


Fig. 5 PDFs of curvature shape factor s_h on the $c = 0.8$ isosurface for all cases
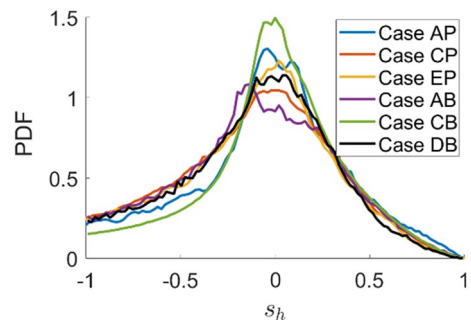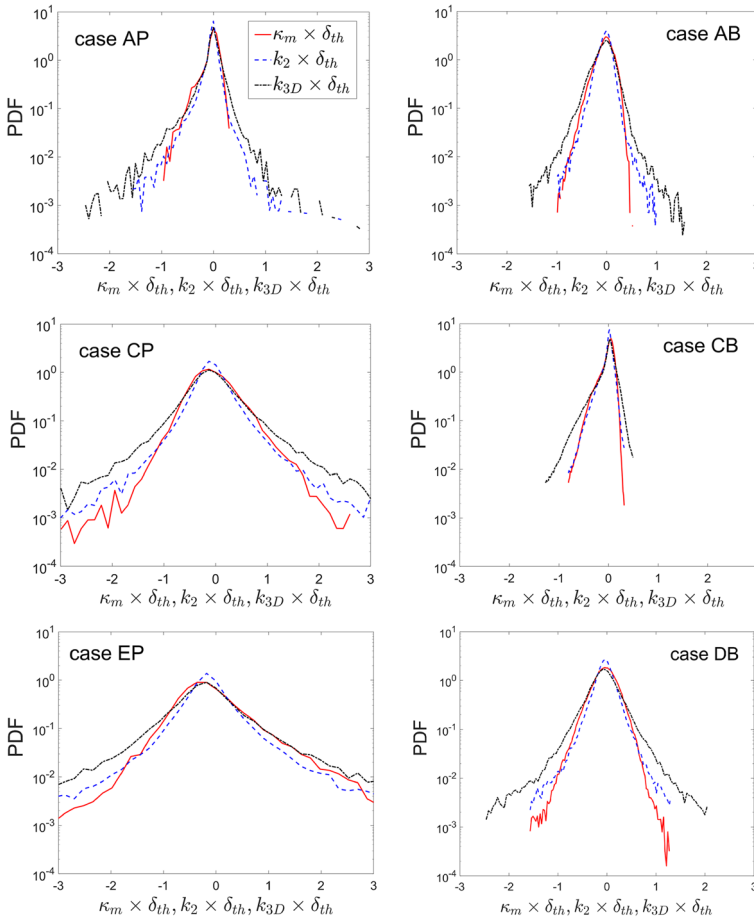
Fig. 6 PDFs of $\kappa_m \times \delta_{th}$, $k_2 \times \delta_{th}$ and $k_{3D} \times \delta_{th} = k_2 \times \pi/2 \times \delta_{th}$ on the $c = 0.8$ isosurface for all cases in semi-log scale

the PDFs of k_{3D} and κ_m, which cannot be ignored. This behaviour is not completely unexpected because of assumptions (e.g., $P(\phi, \alpha, k_2) = P(\phi)P(\alpha)P(k_2)$ and the presumed distributions of $P(\phi)$ and $P(\alpha)$) made while deriving Eq. (11). In order to assess these assumptions, the PDFs of ϕ and α are compared to their presumed distributions for the $c = 0.8$ isosurface in Fig. 7a and b, respectively, exemplarily for cases AP and EP. It can be seen from Fig. 7a and b that the PDFs of ϕ and α (i.e. $P(\phi)$ and $P(\alpha)$) show reasonable agreement with the presumed distributions (i.e. $P(\phi) = (\cos\phi)/2$ and $P(\alpha) = 1/2\pi$) for isotropic distribution of the orientation of $\vec{N}$ in case EP. By contrast, $P(\phi)$ and $P(\alpha)$ extracted from DNS data exhibit significant quantitative differences from the presumed distributions (i.e. $P(\phi) = (\cos\phi)/2$ and $P(\alpha) = 1/2\pi$) in case AP. This suggests that the isotropic relations given by $P(\phi) = (\cos\phi)/2$ and $P(\alpha) = 1/2\pi$ hold more satisfactorily for higher values of u'/S_L, which is consistent with previous findings (Chakraborty and Hawkes 2011; Chakraborty et al. 2013) and the distributions of $P(\phi)$ and $P(\alpha)$ reported by Wang et al. (2021). The same qualitative behaviour has been observed for other c-isosurfaces in cases AP and EP. The Bunsen cases mostly resemble with case AP and thus these results are
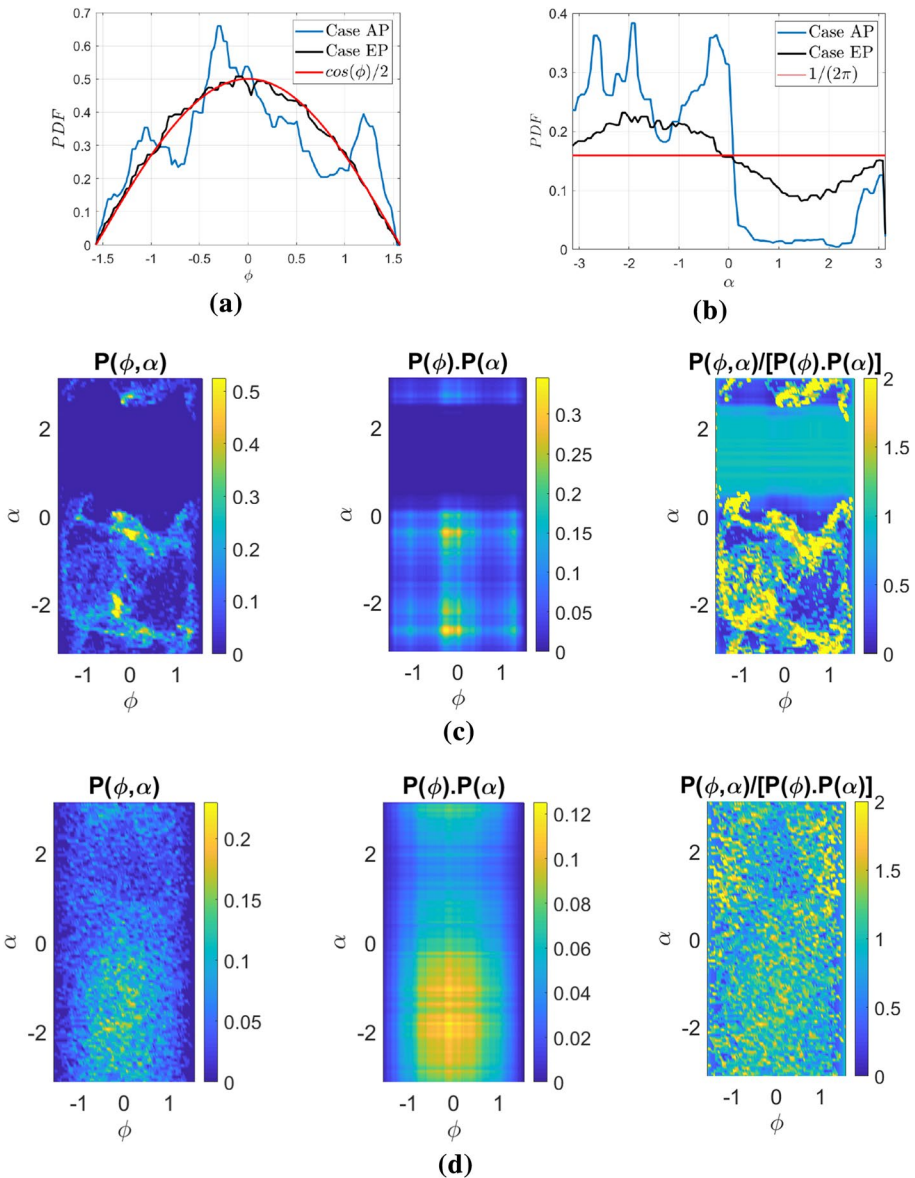
Fig. 7 PDFs of **a** ϕ and **b** α along with their presumed distributions (i.e. $P(\phi) = (\cos\phi)/2$ and $P(\alpha) = 1/(2\pi)$ for the $c = 0.8$ isosurface. Distributions of $P(\phi, \alpha)$, $P(\phi) \cdot P(\alpha)$ and $P(\phi, \alpha)/[P(\phi) \cdot P(\alpha)]$ for the $c = 0.8$ isosurface for cases **c** AP and **d** EP

not explicitly shown here, but the level of agreement with the presumed distributions of $P(\phi)$ and $P(\alpha)$ with DNS data increases from AB to DB. A monotonic trend from case AP to EP is observed for the statistically planar flame cases, as u'/S_L increases. The joint PDF contours of ϕ and α (i.e. $P(\phi, \alpha)$) for the $c = 0.8$ isosurface are shown in Fig. 7c and d for cases AP and EP, respectively. It can be seen from Fig. 7c and d that the correlation

between ϕ and α remains weak (e.g. correlation coefficient is of the order of 0.01), which is consistent with previous findings of Veynante remains weak (e.g. correlation coefficient is of the order of 0.01), whichis consistent with previous findings of Veynante et al. (2010); Hawkes et al. (2011) and Wang et al. (2021). Figure 7c and d also show the corresponding distributions of $P(\phi) \cdot P(\alpha)$ and $P(\phi, \alpha)/[P(\phi) \cdot P(\alpha)]$, which exhibit that $P(\phi) \cdot P(\alpha)$ reasonably captures the qualitative behaviour of $P(\phi, \alpha)$. Moreover, $P(\phi, \alpha)/[P(\phi) \cdot P(\alpha)]$ remains of the order of unity at most locations within the $\phi - \alpha$ space and this situation is more prevalent for higher turbulence intensity cases. These findings are consistent with previous findings of Veynante et al. (2010); Hawkes et al. (2011) and Wang et al. (2021). Once again, the findings from Fig. 7c and d also hold for other c isosurfaces and also for other cases with an increasing probability of obtaining $P(\phi, \alpha)/[P(\phi) \cdot P(\alpha)] \approx 1.0$ with an increase in u'/S_L. Finally, the joint PDF contours of $k_2 \delta_{th}, \phi$ and α (i.e. $P(\phi, \alpha, k_2 \delta_{th})$ for the $c = 0.8$ isosurface for cases AP and EP are shown in Fig. 8 for $\phi = 0^o$ alongside the distributions of $P(\phi) \cdot P(\alpha) \cdot P(k_2 \delta_{th})$ and $P(\phi, \alpha, k_2 \delta_{th})/[P(\phi) \cdot P(\alpha) \cdot P(k_2 \delta_{th})]$. It is worthwhile to note that these distributions are qualitatively similar for other c-isosurfaces for not only cases AP and EP but also for other cases. Figure 8 suggests that α, ϕ and $k_2 \delta_{th}$ are weakly correlated with each other (i.e. correlation coefficients are of the order of 0.001) and $P(\phi) \cdot P(\alpha) \cdot P(k_2 \delta_{th})$ captures the qualitative behaviours of $P(\phi, \alpha, k_2 \delta_{th})$. Moreover, it is evident from Fig. 8 that $P(\phi, \alpha, k_2 \delta_{th})/[P(\phi) \cdot P(\alpha) \cdot P(k_2 \delta_{th})]$ remains close to unity at most locations in the $k_2 - \phi - \alpha$ space. It is worthwhile to note that a weak correlation does not necessarily guarantee statistical independence but the order of unity values of $P(\phi, \alpha)/[P(\phi) \cdot P(\alpha)]$ and $P(\phi, \alpha, k_2 \delta_{th})/[P(\phi) \cdot P(\alpha) \cdot P(k_2 \delta_{th})]$ inspire confidence in terms of validity of statistical independence between k_2, ϕ and α, as a first-order approximation.

It is worthwhile to note that the joint PDFs $P(\phi, \alpha)$ and $P(\phi, \alpha, k_2 \delta_{th})$ are often noisy (not only in this study but also in Chakraborty et al. (2013); Wang et al. (2021)), which can also potentially affect the distributions of $P(\phi, \alpha)/[P(\phi) \cdot P(\alpha)]$ and $P(\phi, \alpha, k_2 \delta_{th})/[P(\phi) \cdot P(\alpha) \cdot P(k_2 \delta_{th})]$ presented in Figs. 7 and 8. The information extracted from Figs. 7 and 8 reveals that the inaccuracy in the parameterisation of $P(\alpha)$ and the local discrepancies between $P(\phi, \alpha)$ and $P(\phi) \cdot P(\alpha)$, and also between $P(\phi, \alpha, k_2 \delta_{th})$ and $P(\phi) \cdot P(\alpha) \cdot P(k_2 \delta_{th})$ contributes to the discrepancies between the prediction of Eq. (11) and κ_m PDFs extracted from DNS data. More information in different configurations will be needed to propose better parameterisations of $P(\alpha), P(\phi, \alpha)$ and $P(\phi, \alpha, k_2 \delta_{th})$, which is beyond the scope of the current analysis but will need further work.

The differences between the PDFs of κ_m and k_{3D} can lead to differences between $\overline{k_{3D}^2} = (\pi/2)^2 \times \overline{k_2^2}$ and $\overline{\kappa_m^2}$, and also between $\overline{k_{3D}^3} = (\pi/2)^3 \times \overline{k_2^3}$ and $\overline{\kappa_m^3}$. The ratios $p_2 = \overline{k_2^2}/\overline{\kappa_m^2}$ and $p_3 = \overline{k_2^3}/\overline{\kappa_m^3}$ for $c = 0.1, 0.5$ and 0.9 are shown in Fig. 9 for all cases considered here. It is important to note that the mean values (i.e., first moments) of k_2 and κ_m assume individually vanishingly small values, and thus their ratio does not offer any physical information and only shows numerical noise. Thus, the ratio of the mean values (i.e., first moments) of k_2 and κ_m will not be discussed further in this paper. It is evident from Fig. 9 that $p_2 = \overline{k_2^2}/\overline{\kappa_m^2}$ remains greater than $9/16 = 0.5625$, which can be obtained according to Eq. (12i) if there is a significant probability of obtaining saddle type curvatures (i.e. $\kappa_1 \kappa_2 < 0$ or $s_h < 0$). It has already been shown in Fig. 5 that there is a significant probability of obtaining saddle type curvatures (i.e., $\kappa_1 \kappa_2 < 0$ or $s_h < 0$) and this contributes to $p_2 = \overline{k_2^2}/\overline{\kappa_m^2} > 0.5625$. Conversely, a value of $p_2 = \overline{k_2^2}/\overline{\kappa_m^2} = 0.5625$ is obtained if the flame only exhibits cylindrical curvatures (i.e., a delta PDF of s_h with an impulse at $s_h = 0$).

Case AP   **Case EP**
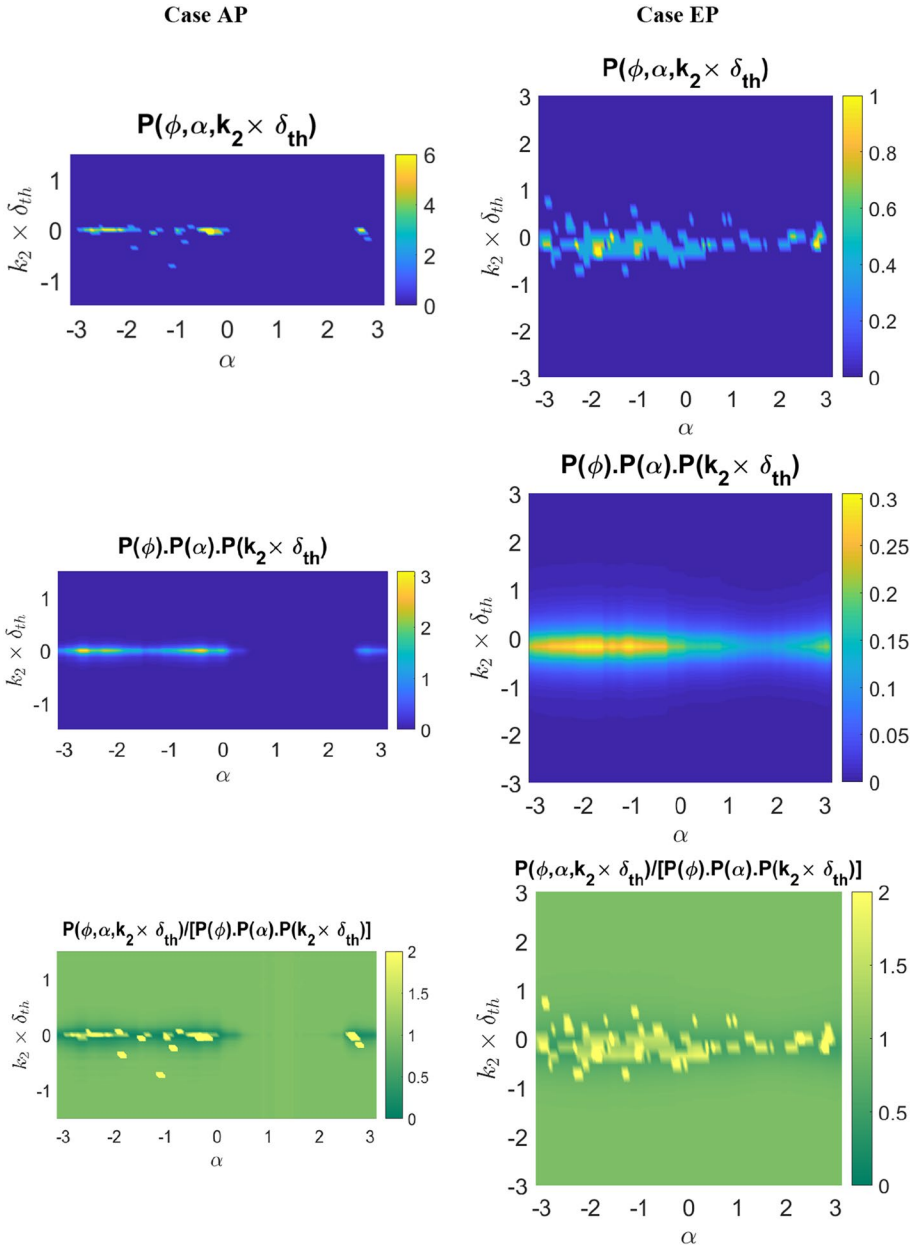
Fig. 8 Distributions of $P(\phi, \alpha, k_2\delta_{th})$, $P(\phi) \cdot P(\alpha) \cdot P(k_2\delta_{th})$ and $P(\phi, \alpha, k_2\delta_{th})/[P(\phi) \cdot P(\alpha) \cdot P(k_2\delta_{th})]$ for the $c = 0.8$ isosurface for $\phi = 0^o$ in cases AP (1st column) and EP (2nd column)

Figure 9 also indicates that $p_3 = \overline{k_2^3}/\overline{\kappa_m^3}$ assumes positive values in all cases, which suggests that the skewness of the PDF of $k_{3D} = k_2 \times \pi/2$ will be able to provide the correct qualitative trend regarding the skewness of the curvature κ_m PDF. This aspect is particularly important because the negative skewness of κ_m is often taken to be a marker of the

Fig. 9 Variations of **a** $p_2 = \overline{k_2^2}/\overline{\kappa_m^2}$ and **b** $p_3 = \overline{k_2^3}/\overline{\kappa_m^3}$ for $c = 0.1, 0.5$ and 0.9 for all cases
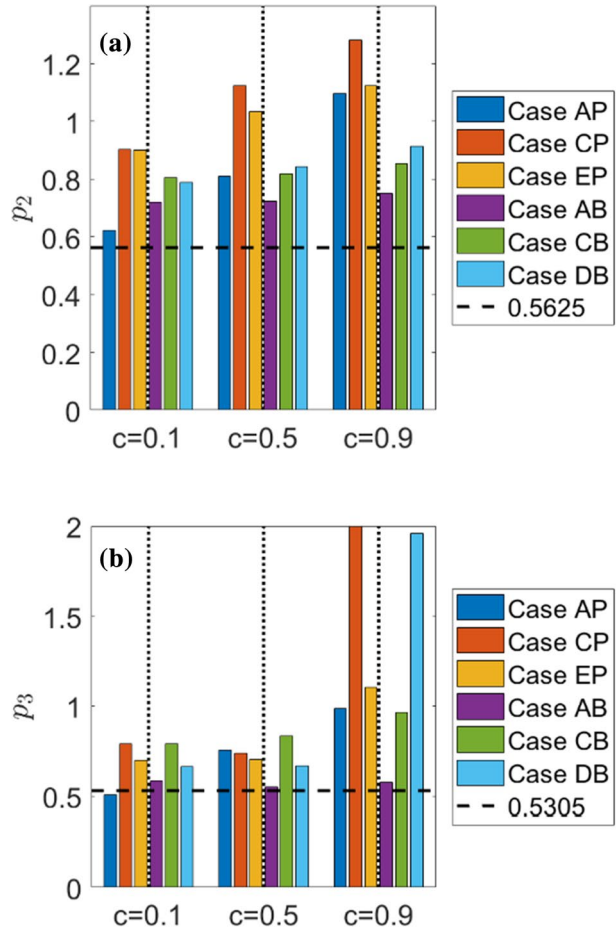
Darrieus-Landau instability (Creta et al. 2016; Klein et al. 2018a). It is also evident from Fig. 9 that the value of $p_3 = \overline{k_2^3}/\overline{\kappa_m^3}$ remains mostly greater than $5/3\pi = 0.5305$ for all cases. This behaviour can also be expected from Eq. (12ii) because of the significant probability of obtaining saddle type flame topologies (i.e., $\kappa_1 \kappa_2 < 0$ or $s_h < 0$) and a value of $p_3 = \overline{k_2^3}/\overline{\kappa_m^3} = 0.5305$ is realised for a purely cylindrical surface.

This behaviour of $p_2 = \overline{k_2^2}/\overline{\kappa_m^2}$ and $p_3 = \overline{k_2^3}/\overline{\kappa_m^3}$ also suggests that even though the approximation given by Eq. (11) (i.e. $P(k_2) \times 2/\pi = P(\kappa_m)$ and $P(k_2)dk_2 = P(\kappa_m)d\kappa_m$) captures the general shape of the PDF of κ_m, the moments of κ_m may not be adequately captured by the corresponding moments of two-dimensional measurements of flame curvature. However, positive values of $p_3 = \overline{k_2^3}/\overline{\kappa_m^3}$ suggest that the skewness of the actual curvature PDF could at least be qualitatively captured by the corresponding value obtained from its two-dimensional equivalent, provided the measurement plane includes the mean direction of flame propagation. Although the ratio of second and third moments of curvature in two- and three-dimensions can be estimated for pure cylindrical surfaces from Eqs. (12i) and (12ii) subject to the assumptions of isotropy, the actual ratios for premixed flame surfaces remain greater than the values for cylindrical surfaces due to the significant
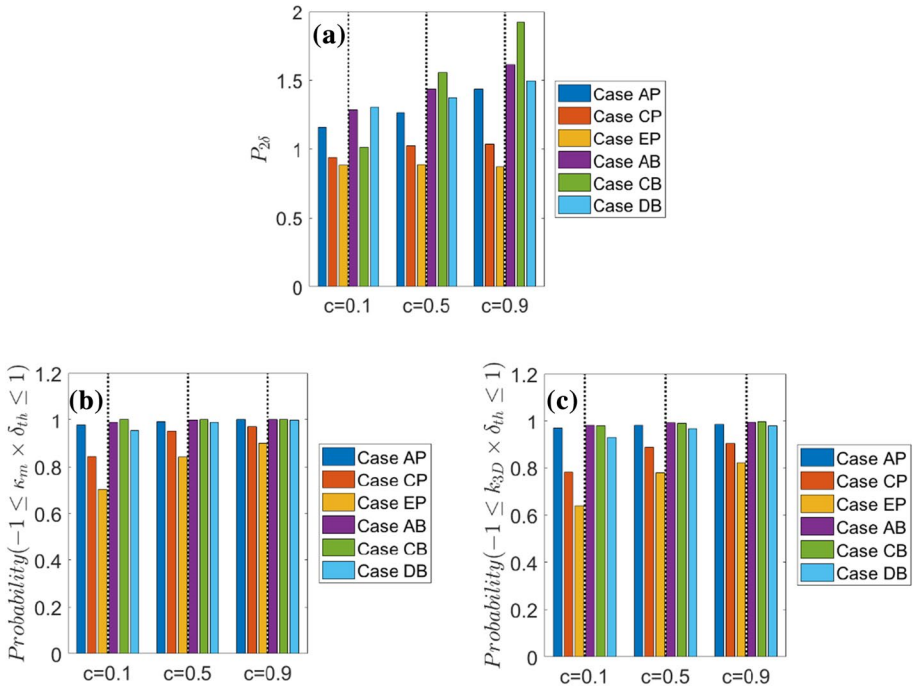
Fig. 10 Variations of **a** $p_{2\delta}$, **b** $\int_{-1/\delta_{th}}^{1/\delta_{th}} P(\kappa_m)d\kappa_m$ and **c** $\int_{-1/\delta_{th}}^{1/\delta_{th}} P(k_{3D})dk_{3D}$ for $c = 0.1, 0.5$ and 0.9 for all cases

presence of saddle type (i.e., $\kappa_1\kappa_2 < 0$) flame topologies. The performance of the approximation given by Eq. (11) to predict the second moment of curvature within the ranges given by $-1/\delta_{th} \leq \kappa_m \leq 1/\delta_{th}$ and $-1/\delta_{th} \leq k_{3D} \leq 1/\delta_{th}$ can be quantified by:

$$p_{2\delta} = \int_{-1/\delta_{th}}^{1/\delta_{th}} k_{3D}^2 P(k_{3D})dk_{3D} \bigg/ \int_{-1/\delta_{th}}^{1/\delta_{th}} \kappa_m^2 P(\kappa_m)d\kappa_m \text{ with } P(k_{3D}) = 2/\pi \times P(k_2) \quad (15)$$

It can be seen from Fig. 10 that the ratio of $\int_{-1/\delta_{th}}^{1/\delta_{th}} k_{3D}^2 P(k_{3D})dk_{3D}$ and $\int_{-1/\delta_{th}}^{1/\delta_{th}} \kappa_m^2 P(\kappa_m)d\kappa_m$ (i.e. $p_{2\delta} = \int_{-1/\delta_{th}}^{1/\delta_{th}} k_{3D}^2 P(k_{3D})dk_{3D} \bigg/ \int_{-1/\delta_{th}}^{1/\delta_{th}} \kappa_m^2 P(\kappa_m)d\kappa_m$ with $P(k_{3D}) = 2/\pi \times P(k_2)$) remains close to unity and the probabilities of finding $-1/\delta_{th} \leq \kappa_m \leq 1/\delta_{th}$ and $-1/\delta_{th} \leq k_{3D} \leq 1/\delta_{th}$ (i.e. $\int_{-1/\delta_{th}}^{1/\delta_{th}} P(\kappa_m)d\kappa_m$ and $\int_{-1/\delta_{th}}^{1/\delta_{th}} P(k_{3D})dk_{3D}$) remain comparable and include at least 70% of the samples for the range of turbulence intensities considered here. The magnitudes of both $\int_{-1/\delta_{th}}^{1/\delta_{th}} k_{3D}^3 P(k_{3D})dk_{3D}$ and $\int_{-1/\delta_{th}}^{1/\delta_{th}} \kappa_m^3 P(\kappa_m)d\kappa_m$ remain at least one order of magnitude smaller than $\int_{-\infty}^{\infty} k_{3D}^3 P(k_{3D})dk_{3D}$ and $\int_{-\infty}^{\infty} \kappa_m^3 P(\kappa_m)d\kappa_m$, respectively except for case AP where these values are comparable. Moreover, both $\int_{-1/\delta_{th}}^{1/\delta_{th}} \delta_{th}^3 k_{3D}^3 P(k_{3D}\delta_{th})dk_{3D}$ and $\int_{-1/\delta_{th}}^{1/\delta_{th}} \delta_{th}^3 \kappa_m^3 P(\kappa_m\delta_{th}^3)d\kappa_m$ assume magnitudes much smaller

than 0.01 in other cases, and thus their ratio provides numerical noise instead of any physical insights and thus is not explicitly shown in Fig. 10. The findings from Fig. 10 suggest that the approximation given by Eq. (11) can be used to obtain the three-dimensional curvature statistics in terms of its probability and second moment within the range given by $-1/\delta_{th} \leq k_{3D} \leq 1/\delta_{th}$ and the agreement between k_{3D} and κ_m statistics improves with decreasing window size around the mean value (not shown here). It is worth noting that a log-normal PDF distribution is often used to approximate the PDF of the scalar dissipation rate in passive scalar despite well-known discrepancy between the actual distribution and log-normal distribution at the tails of the PDFs (Markides and Chakraborty 2013). By the same token, Eq. (11) is expected to approximate PDF of κ_m for the curvature range which includes at least 70% of the sample points for the range of turbulence parameters considered here.

5 Conclusions

In the present analysis, a transformation, which relates the actual flame curvature PDF evaluated in three-dimensions with the curvature evaluated based on two-dimensional flame contours, has been derived based on the assumption of the isotropic distribution of ϕ (the angle between the flame normal vector and the measurement plane) and statistical independence of various angles and two-dimensional curvature. The relation between the PDF of actual three-dimensional curvature and the PDF resulting from two-dimensional evaluation of curvature has been assessed based on DNS databases of turbulent premixed (a) statistically planar and (b) statistically axisymmetric Bunsen flames. It has been found that the analytically derived relation between the PDFs of actual three-dimensional curvature and the corresponding two-dimensional evaluation of curvature holds reasonably well for a range of different turbulence intensities across different combustion regimes. It has been shown that the flame surface shows predominantly two-dimensional cylindrical curvature but there is a significant probability of finding saddle type flame topologies. The presence of saddle type flame topologies significantly affects the ratios of second and third moments of two-dimensional and three-dimensional curvatures. It has been found that the ratios of second and third moments of two-dimensional and three-dimensional curvatures cannot be accurately predicted by assuming only two-dimensional cylindrical curvature distribution. Moreover, it was demonstrated by Hawkes et al. (2011); Veynante et al. (2010) that the assumptions of isotropic distributions of ϕ and α yield a relation between the surface-averaged 3D curvature $\overline{(\kappa_m)}_s = \overline{\kappa_m |\nabla c|}/\overline{|\nabla c|}$ and its two-dimensional counterpart $\overline{(k_2)}_{s2} = \overline{k_2 |\nabla c|_{2D}}/\overline{|\nabla c|_{2D}}$ as: $\overline{(\kappa_m)}_s = 2/\pi \overline{(k_2)}_{s2}$ where $|\nabla c|_{2D}$ is the 2D measurement of $|\nabla c|$ based on the projection of scalar gradient on the measurement plane. The validity of the relation $\overline{(\kappa_m)}_s = \pi/2 \overline{(k_2)}_{s2}$ has been established based on DNS data (Hawkes et al. 2011; Veynante et al. 2010; Wang et al. 2021), and a similar expression $\overline{(\kappa_m)} = \pi/2 \overline{(k_2)}$ can be obtained using Eqs. (6) and (11) along with $P(\phi) = (cos\phi)/2$ and $P(\alpha) = 1/2\pi$. This indicates that the assumptions of isotropy of ϕ and α are sufficient for first-order moments of curvature, which is necessary for the FSD based turbulent premixed flame modelling (Hawkes et al. 2011; Veynante et al. 2010; Chakraborty and Hawkes 2011; Wang et al. 2021). However, irrespective of the validity of these assumptions and the

statistical independence of ϕ, α and k_2 (i.e. $P(\phi, \alpha, k_2) = P(\phi)P(\alpha)P(k_2)$), the Gauss curvature $\kappa_1\kappa_2$ plays a role in determining $\overline{k_2^2}/\overline{\kappa_m^2}$ and $\overline{k_2^3}/\overline{\kappa_m^3}$ according to Eqs. (13i–13ii). This has important implications because the second-moment of curvature plays a key role in terms of determining the curvature stretch contribution to the FSD transport (Chakraborty and Cant 2007, 2009; Wang et al. 2021), whereas the third-moment of curvature is often used for the purpose of characterising the Darrius-Landau instability (Creta et al. 2016; Klein et al. 2018a). However, despite the quantitative differences between the third moments of two-dimensional and three-dimensional curvatures, their ratio remains positive and thus the qualitative nature of curvature skewness can still be obtained based on two-dimensional curvature measurements. As the curvature skewness is often taken to be a marker of the Darrius-Landau instability, the conclusion regarding the presence of this instability can potentially be taken from the two-dimensional curvature measurements. Therefore, two-dimensional experimental measurements are expected to provide the correct qualitative behaviours in terms of curvature statistics and its application to the evaluation of the curvature contributions to the FSD transport and for the identification and characterisation of the Darrius-Landau instability.

The assumptions of isotropic distributions of ϕ and α used to derive Eq. (11) have been utilised in the past to propose correction factors for the planar measurements of the FSD and scalar dissipation rate transport equations to obtain their actual three-dimensional counterparts (Hawkes et al. 2011; Veynante et al. 2010; Chakraborty and Hawkes 2011; Chakraborty et al. 2013; Wang et al. 2021). The approximation of the three-dimensional curvature distribution from 2D measurements and its associated limitations will enable experimentalists to estimate the Markstein length (e.g. curvature dependence of flame displacement speed $S_d = |\nabla c|^{-1}(Dc/Dt)$) (Peters et al. 1998; Chakraborty and Cant 2004; Chakraborty 2007) and flame stretch rate due to flame curvature (i.e. $2S_d\kappa_m$) (Wang et al. 2021)) for the purpose of the development of new models and their assessments.

Although the transformation given by Eq. (11) holds reasonably well for statistically planar flames and Bunsen burner flames, more analysis in other configurations will be necessary. Moreover, the validity of Eq. (11) needs to be assessed for a wider range of turbulence intensity than the range considered in the present analysis. While the nature of thermo-chemistry is unlikely to affect the conclusions of the present analysis, the current findings need to be validated with respect to detailed chemistry DNS data. Finally, it will be ideal to have simultaneous both 2D and 3D measurements of curvature for an experimental dataset to assess the relations derived here. Such information is rare in the existing literature but will serve as an ideal testbed for the relations derived here.

Declarations

Conflict of interest The authors complied with all ethical standards relevant to this work. The authors declare that they have no conflict of interest.

References

Ahmed, U., Chakraborty, N., Klein, M.: Insights into the bending effect in premixed turbulent combustion using the Flame Surface Density transport. Combust. Sci. Technol. **191**, 898–920 (2019a)

Ahmed, U., Klein, M., Chakraborty, N.: On the stress-strain alignment in premixed turbulent flames. Sci. Rep. **9**, 5092 (2019b)

Ahmed, U., Herbert, A., Chakraborty, N., Klein, M.: On the validity of Damköhler's second hypothesis in statistically planar turbulent premixed flames in the thin reaction zones regime. Proc. Combust. Inst. **38**, 3039–3047 (2021)

Anselmo-Filho, P., Hochgreb, S., Barlow, R.S., Cant, R.S.: Experimental measurements of geometric properties of turbulent stratified flames. Proc. Combust. Inst. **32**, 1763–1770 (2009)

Bradley, D., Gaskell, P.H., Sedaghat, A., Gu, X.J.: Generation of PDFS for flame curvature and for flame stretch rate in premixed turbulent combustion. Combust. Flame **135**, 503–523 (2003)

Chakraborty, N.: Comparison of displacement speed statistics of turbulent premixed flames in the regimes representing combustion in corrugated flamelets and the thin reaction zones. Phys. Fluids **19**, 105109 (2007)

Chakraborty, N., Cant, S.: Unsteady effects of strain rate and curvature on turbulent premixed flames in an inflow–outflow configuration. Combust. Flame **137**, 129–147 (2004)

Chakraborty, N., Cant, R.S.: Statistical behaviour and modelling of flame normal vector in turbulent premixed flames. Num. Heat Trans. A **50**, 623–643 (2006)

Chakraborty, N., Cant, R.S.: A-priori analysis of the curvature and propagation terms of the flame surface density transport equation for large eddy simulation. Phys. Fluids **19**, 105101 (2007)

Chakraborty, N., Cant, R.S.: Direct numerical simulation analysis of the flame surface density transport equation in the context of large eddy simulation. Proc. Combust. Inst. **32**, 1445–1453 (2009)

Chakraborty, N., Hawkes, E.R.: Determination of 3D flame surface density variables from 2D measurements: validation using direct numerical simulation. Phys. Fluids **23**, 065113 (2011)

Chakraborty, N., Champion, M., Mura, A., Swaminathan, N.: Scalar Dissipation Rate Approach to Reaction Rate Closure Turbulent Premixed Flame, pp. 74–102. Cambridge University Press, Cambridge, UK (2011a)

Chakraborty, N., Hartung, G., Katragadda, M., Kaminski, C.F.: A numerical comparison of 2D and 3D density-weighted displacement speed statistics and implications for laser based measurements of flame displacement speed. Combust. Flame **158**, 1372–1390 (2011b)

Chakraborty, N., Kolla, H., Sankaran, R., Hawkes, E.R., Chen, J.H., Swaminathan, N.: Determination of three-dimensional quantities related to scalar dissipation rate and its transport from two-dimensional measurements: direct Numerical Simulation based validation. Proc. Combust. Inst. **34**, 1151–1162 (2013)

Chakraborty, N., Alwazzan, D., Klein, M., Cant, R.S.: On the validity of Damköhler's first hypothesis in turbulent Bunsen burner flames: a computational analysis. Proc. Combust. Inst. **37**, 2231–2239 (2019)

Chakraborty, N., Klein, M., Im, H.G.: A comparison of entrainment velocity and displacement speed statistics in different regimes of turbulent premixed combustion. Proc. Combust. Inst. **38**, 2985–2992 (2020)

Chen, Y.C., Bilger, R.W.: Experimental investigation of three-dimensional flame-front structure in premixed turbulent combustion—I: hydrocarbon/air bunsen flames. Combust. Flame **131**, 400–435 (2002)

Chen, Y.C., Kim, M., Han, J., Yun, S., Yoon, Y.: Measurements of the heat release rate integral in turbulent premixed stagnation flames with particle image velocimetry. Proc. Combust. Inst. **31**, 1327–1335 (2007)

Cifuentes, L., Kempf, A.M., Dopazo, C.: Local entrainment velocity in a premixed turbulent annular jet flame. Proc. Combust. Inst. **37**, 2493–2501 (2019)

Creta, F., Lamioni, R., Lapenna, P.E., Troiani, G.: Interplay of Darrieus-Landau instability and weak turbulence in premixed flame propagation. Phys. Rev. E **94**, 053102 (2016)

Echekki, T., Chen, J.H.: Unsteady strain rate and curvature effects in turbulent premixed methane-air flames. Combust. Flame **116**, 184–202 (1996)

Gashi, S., Hult, J., Jenkins, K.W., Chakraborty, N., Cant, R.S., Kaminski, C.F.: Curvature and wrinkling of premixed flame kernels—comparisons of OH PLIF and DNS data. Proc. Combust. Inst. **30**, 809–817 (2005)

Hawkes, E.R., Cant, R.S.: A flame surface density approach to large eddy simulation of premixed turbulent combustion. Proc. Combust. Inst. **28**, 51–58 (2000)

Hawkes, E.R., Sankaran, R., Chen, J.H.: Estimates of the three-dimensional Flame Surface Density and every term in its transport equation from two-dimensional measurements. Proc. Combust. Inst. **33**, 1447–1454 (2011)

Jenkins, K. W., Cant, R. S.: DNS of turbulent flame kernels. In: Liu, C., Sakell, L., Beautner, T. (eds.), Proc. 2nd AFOSR Conf. on DNS and LES, pp. 192–202. Kluwer Academic Publishers, (1999).

Keil, F.B., Amzehnhoff, M., Chakraborty, N., Klein, M.: Comparison of flame propagation statistics extracted from DNS based on simple and detailed chemistry Part 2: influence of choice of reaction progress variable. Energies **14**, 5695 (2021)

Klein, M., Sadiki, A., Janicka, J.: A digital filter based generation of inflow data for spatially developing direct numerical or large eddy simulations. J. Comp. Phys. **186**, 652–665 (2003)

Klein, M., Chakraborty, N., Ketterl, S.: A comparison of strategies for Direct Numerical Simulation of turbulence chemistry interaction in generic planar turbulent premixed flames. Flow Turb. Combust. **199**, 955–971 (2017)

Klein, M., Nachtigal, H., Hansinger, M., Pfitzner, M., Chakraborty, N.: Flame curvature distribution in high pressure turbulent Bunsen premixed flames, Flow. Turb. Combust. **101**, 1173–1187 (2018a)

Klein, M., Alwazzan, D., Chakraborty, N.: A Direct Numerical Simulation analysis of pressure variation in turbulent premixed Bunsen burner flames - Part 1: scalar gradient and strain rate statistics. Comput. Fluids **173**, 178–188 (2018b)

Knaus, D.A., Sattler, S.S., Gouldin, F.C.: Three-dimensional temperature gradients in premixed turbulent flamelets via crossed-plane Rayleigh imaging. Combust. Flame **141**, 253–270 (2005)

Lachaux, T., Halter, F., Chauveau, C., Gokalp, I., Shepherd, I.G.: Flame front analysis of high-pressure turbulent lean premixed methane–air flames. Proc. Combust. Inst. **30**, 819–826 (2005)

Markides, C.N., Chakraborty, N.: Statistics of the scalar dissipation rate using Direct Numerical Simulations and Planar Laser-Induced Fluorescence data. Chem. Engg. Sci. **90**, 221–241 (2013)

Peters, N.: Turbulent Combustion. Cambridge University Press, Cambridge (2000)

Peters, N., Terhoeven, P., Chen, J.H., Echekki, T.: Statistics of flame displacement speeds from computations of 2-D unsteady methane-air flames. Proc. Combust. Inst. **27**, 833–839 (1998)

Poinsot, T., Lele, S.K.: Boundary conditions for direct simulation of compressible viscous flows. J. Comp. Phys. **101**, 104–129 (1992)

Poinsot, T., Veynante, D.: Theoretical and Numerical Combustion. R.T. Edwards Inc., Philadelphia, USA (2001)

Poinsot, T., Echekki, T., Mungal, M.: A study of the laminar flame tip and implications for turbulent premixed combustion. Combust. Sci. Tech. **81**, 45–73 (1992)

Renou, B., Boukhalfa, A., Peuchberty, D., Trinité, M.: Effects of stretch on the local structure of freely propagating premixed low-turbulent flames with various Lewis numbers. Proc. Combust. Inst. **27**, 841–847 (1998)

Sankaran, R., Hawkes, E.R., Chen, J.H., Lu, T.H., Law, C.K.: Structure of a spatially developing turbulent lean methane-air Bunsen flame. Proc. Combust. Inst. **31**, 1291–1298 (2007)

Shepherd, I.G., Ashurst, W.T.: Flame front geometry in premixed turbulent flames. Proc. Combust. Inst. **24**, 485–491 (1992)

Shepherd, I.G., Cheng, R.K.: The burning rate of premixed flames in moderate and intense turbulence. Combust. Flame **127**, 2066–2075 (2001)

Shy, S.S., Lee, W.K.E.I., Yang, T.S.: Experimental analysis of flame surface density modeling for premixed turbulent combustion using aqueous autocatalytic reactions. Combust. Flame **118**, 606–618 (1999)

Shy, S.S., Lee, E.I., Chang, N.W., Yang, S.I.: Direct and indirect measurements of flame surface density, orientation, and curvature for premixed turbulent combustion modeling in a cruciform burner. Proc. Combust. Inst. **28**, 383–390 (2000)

Steinberg, A.M., Driscoll, J.F.: Stretch-rate relationships for turbulent premixed combustion LES subgrid models measured using temporally resolved diagnostics. Combust. Flame **156**, 2285–2306 (2009)

Veynante, D., Lodato, G., Domingo, P., Vervisch, L., Hawkes, E.R.: Estimation of three-dimensional flame surface densities from planar images in turbulent premixed combustion. Exp. Fluids **49**, 267–278 (2010)

Wang, H., Hawkes, E.R., Ren, J., Chen, G., Luo, K., Fan, J.: 2D and 3D measurements of flame stretch and turbulence-flame interactions in turbulent premixed flames using DNS. J. Fluid Mech. **913**, A11 (2021)